Hyperfine Interactions (2019) 240:117
https://doi.org/10.1007/s10751-019-1678-4

Characterization of *Mycobacterium tuberculosis* ferredoxin with Mössbauer spectroscopy

Christina S. Müller[1] · Dominique F. Bechtel[2] · Hendrik Auerbach[1] · Juliusz A. Wolny[1] · Antonio J. Pierik[2] · Volker Schünemann[1]

Published online: 18 November 2019

Abstract
A Mössbauer spectroscopic characterization of *Mycobacterium tuberculosis* ferredoxin (*Mt* Fdx) CNL73887.1 has been performed. In the Mössbauer spectrum obtained at $T = 77$ K two components in a 1:2 ratio are present: The minority component **1** possesses $\delta_1 = 0.27$ (± 0.02) mms^{-1} and $\Delta E_{Q1} = -0.53$ (± 0.03) mms^{-1}. The majority component **2** shows $\delta_2 = 0.44$ (± 0.02) mms^{-1} and $\Delta E_{Q2} = 1.47$ (± 0.03) mms^{-1}. This parameter set is characteristic for one Fe^{3+} ion and two $Fe^{2.5+}$ ions present in a $[3Fe\text{-}4S]^0$-cluster. In external magnetic fields of $B = 100$ mT and $B = 5$ T *Mt* Fdx shows a paramagnetic behaviour. Analysis of the field dependent spectra by means of the spin Hamilton formalism, assuming a total spin of $S = 2$, clearly shows that *Mt* Fdx contains a paramagnetic $[3Fe\text{-}4S]^0$-cluster. The experimental results are compared to density functional theory calculations based on a crystal structure of a *Rhodopseudomonas palustris* (*Rp*) HaA2 Fdx (pdb: 4OV1) embedded in a box of water. The addition of explicit solvent molecules showed significant improvement of the accordance of calculated and experimentally obtained hyperfine parameters compared to the calculation in vacuum.

Keywords *M. tuberculosis* Ferredoxin · [3Fe-4S]-cluster · Mössbauer spectroscopy · DFT calculations

This article is part of the Topical Collection on *Proceedings of the International Conference of the Application of the Mössbauer Effect (ICAME 2019) held in Dalian, China, 1-6 September 2019*
Edited by Tao Zhang, Junhu Wang and Xiaodong Wang

Electronic supplementary material The online version of this article (https://doi.org/10.1007/s10751-019-1678-4) contains supplementary material, which is available to authorized users.

✉ Christina S. Müller
csmueller@physik.uni-kl.de

Antonio J. Pierik
pierik@chemie.uni-kl.de

Extended author information available on the last page of the article

1 Introduction

Ferredoxins (Fdx) contain a wide range of iron-sulfur (FeS)-cluster types from [2Fe-2S]- over [3Fe-4S]- to [4Fe-4S]-clusters. The variable oxidation state of these clusters enables Fdx to transfer electrons in numerous biological processes. [1] In bacteria a highly evolved cytochrome P450 mono-oxygenase (CYP) complement, which typically involves Fdx as a redox partner, is essential for the survival of the organism [2–5]. Ensuring the viability of the human pathogen *Mycobacterium tuberculosis* (*Mt*), CYP-enzymes are targets for the development of new anti-tuberculosis drugs [4, 5]. Due to the growing number of multiresistant strains of *Mt*, tuberculosis again threatens to become a serious health risk both in industrial and developing countries [2, 4]. The characterization of putative CYP redox partners such as Fdx is essential to perform P450 activity tests in order to develop possible inhibitors of the CYP system [6]. However, only few Fdx were characterized in the context of the CYP system so far [4, 6].

In bacteria there is a distinct sequence similarity in the cluster-binding motif of Fdx: Cys-X-X-X-X-X-Cys-$(X)_n$-Cys-Pro. In this case X can be replaced by an arbitrary amino acid while $(X)_n$ stands for a spacer of n amino acids [2, 3]. The three conserved cysteines (Cys) are ligands of the iron ions present in the FeS-clusters bound to the protein. If the protein binds a [3Fe4S]-cluster X is usually a glycine or an alanine [3]. In case of a [4Fe-4S]-cluster X is typically replaced by a fourth Cys-residue [2, 3]. *Mt* Fdx CNL73887.1 shows a histidine (His) at the X-position in the cluster-binding motif similar to Fdx of *Rhodopseudomonas palustris* HaA2 (*Rp*) (pdb: 4OV1) [3]. The same appearance of His occurs in Fdx of several other *Mycobacterium* species [4, 5, 7, 8].

It was shown that *Mt* Fdx Rv0763c, *Rp* HaA2 Fdx and *Mt* Fdx Rv1786 exhibit similar spectroscopic features and contain a [3Fe-4S]-cluster [2–4]. In the following study Mössbauer spectroscopy is used as a selective tool to characterize the FeS-cluster present in *Mt* Fdx CNL73887.1. Further insights into the cluster structure and its electronic properties can be gained by density functional theory (DFT) calculations based on X-ray crystal structure data of *Rp* Fdx (pdb: 4OV1) [3] due to the high sequence homology between *Mt* Fdx and *Rp* Fdx.

2 Materials and methods

Full-length *Mt* Fdx CNL73887.1 derived from a codon-optimized synthetic gene (Thermo Fisher Scienfic, Invitrogen) was cloned into the the NcoI and SalI restriction sites of a pET-28a plasmid resulting in an untagged version of the protein. *Mt* Fdx CNL73887.1 was expressed in *Escherichia coli* cells (BL21) and transformed with the pRKISC plasmid for improved FeS incorporation. At 37 °C the bacteria were grown to an OD_{600} of ~ 0.5 in 25 g/l lysogeny broth (LB) medium, induced with 0.5 mM IPTG and incubated at 20 °C overnight. ^{57}Fe powder (33.5 mg) was dissolved in 1 ml HCl (8 M) with 0.59 mmol of sodium citrate for enrichment of the *Mt* Fdx Mössbauer samples with ^{57}Fe. The pH of the solution was adjusted to 5–6 with ammonia. An end concentration of 100 μM Fe in LB medium was used. Purification and concentration of *Mt* Fdx were performed anaerobically via anion exchange chromatography (Q Sepharose Fast Flow, elution at 0.3–0.4 M NaCl), Vivaspin membrane filtration to ~900 μl and gel permeation chromatography in 50 mM HEPES/NaOH pH 8.0 with 100 mM NaCl (HiLoad 26/60 Superdex 75 prep grade, GE Healthcare). The as isolated protein solution (400 μl, 1.4 mM protein with 94% ^{57}Fe enrichment) at pH 8.0 was transferred to a Mössbauer sample holder and frozen at 77 K.

A conventional Mössbauer spectrometer operating in constant acceleration mode in conjunction with a 512-channel analyzer in the time-scale mode (WissEl GmbH) was used to obtain Mössbauer spectra in transmission mode. A sample temperature of $T = 77$ K was maintained using a nitrogen flow cryostat (Optistat^{DN}, Oxford Instruments). Field-dependent Mössbauer spectroscopy at $T = 4.2$ K was performed in a spectrometer equipped with a helium closed-cycle cryostat (CRYO Industries of America Inc.) and a superconducting magnet. The magnetic field was aligned parallel to the direction of γ-rays. All isomer shifts are given relative to α-iron foil measured at room temperature. The raw data were transferred from the multi-channel analyzer to a PC for further analysis employing the public domain program Vinda running on an Excel 2003® platform [9]. Analysis of the 77 K spectra was performed by least-squares fits using Lorentzian line shapes with the linewidth Γ. Simulations of the field-dependent spectra were performed by means of the spin Hamilton formalism [10]. Origin 2017 was used to graphically display the spectra.

DFT calculations of a 'physiological' model (X-ray crystal structure of reduced *Rp* Fdx (pdb: 4OV1) embedded in a cubic box (volume of 125 nm^3) filled with water molecules (density of 998.135 gl^{-1}, simple point charge water spc216.gro) within the Gromacs program package [11]) are presented. Before calculating the Mössbauer parameters with the ORCA program package [12] a geometry optimization of the crystal structure within the water box was performed via GAUSSIAN 16 [13]. Applying the ONIOM method [14] the model was separated into two zones. The FeS-cluster with the Cys-ligands was treated with DFT applying the unrestricted TPSSh functional in combination with the basis set TZV(P) while the remaining protein and all water molecules were treated with molecular mechanics using the universal force field UFF. A stability analysis performed after geometry optimization confirmed that the wavefunction was stable. The calculation of the isomer shift δ and the quadrupole splitting ΔE_Q with ORCA was performed by means of the broken symmetry approach with TPSSh in combination with the basis sets TZV(P)/CP(PPP).

3 Results and discussion

In order to characterize the FeS-cluster in *Mt* Fdx, Mössbauer spectroscopy was performed both at $T = 77$ K and at $T = 4.2$ K in external magnetic fields of $B = 100$ mT and $B = 5$ T. The Mössbauer spectra are shown in Fig. 1 with the parameters listed in Table 1. Component **1**, representing 33% of the relative area, exhibits parameters typical for a high spin ($S = 5/2$) Fe^{3+} ion in a tetrahedral sulfur environment [16]. The major component **2** (67% relative area) shows parameters characteristic for $Fe^{2.5+}$ as present in $[4Fe\text{-}4S]^{2+}$-clusters containing two pairs of $Fe^{2.5+}$ ions each sharing a delocalized electron [16]. The presence of diamagnetic species such as $[4Fe\text{-}4S]^{2+}$- or $[2Fe\text{-}2S]^{2+}$-clusters can be ruled out due to the paramagnetic splitting visible in the field-dependent spectra (see Fig. 1b and c). Figure 1b shows that the application of a weak magnetic field of $B = 100$ mT leads to a magnetic splitting. This behaviour is in line with field-dependent Mössbauer studies of *Desulfovibrio gigas* (*Dg*) Fdx II, and *Azotobacter vinelandii* Fdx both possessing a $[3Fe\text{-}4S]^0$-cluster with a total spin of $S = 2$ [15, 17, 18]. In these systems the electronic relaxation rate is slow compared to the Mössbauer timescale [15, 17, 19]. Hence the analysis of the field-dependent spectra was conducted via the spin Hamilton formalism in the slow relaxation regime assuming a total spin of $S = 2$. The hyperfine coupling constants (A_{xx}, A_{yy}, A_{zz}) exhibit opposite signs for component **1** and **2** (see Table 1) as reported for *Dg* FdxII [15] and the $[3Fe\text{-}4S]^0$-cluster present in benzoyl-coenzyme A epoxidase from

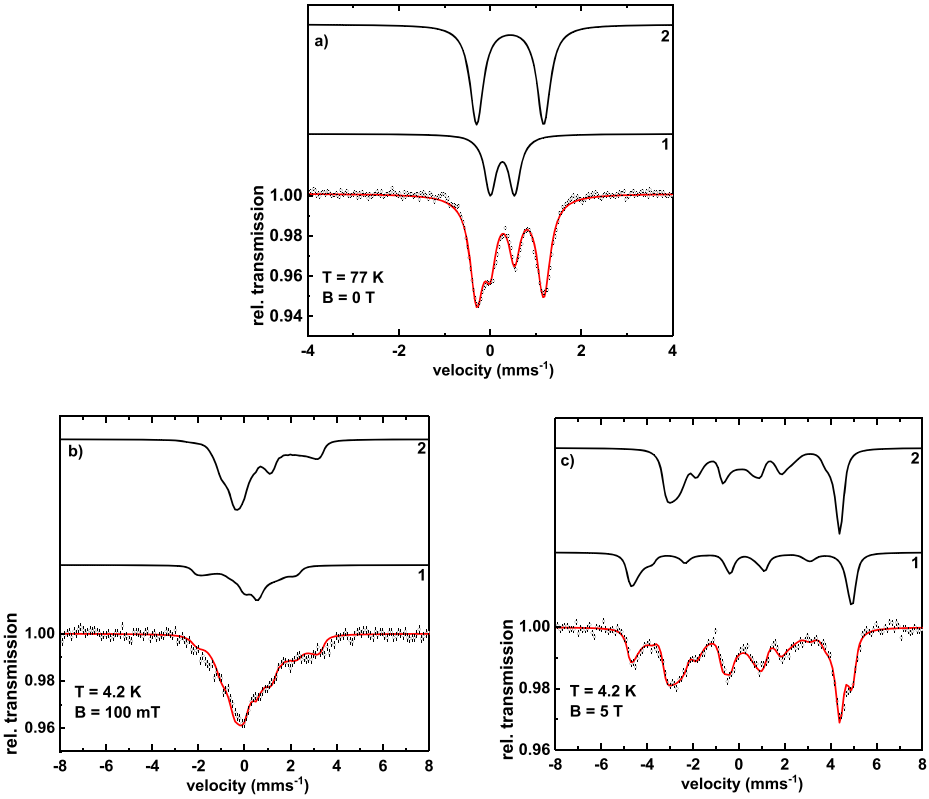

Fig. 1 Mössbauer spectra taken at 77 K of *Mt* Fdx **a**) and at $T = 4.2$ K with an external magnetic field of $B = 100$ mT **b**) and $B = 5$ T **c**) applied parallel to the γ-beam. The simulation (red line) consists of two subcomponents **1** and **2** (black lines) with the Mössbauer parameters listed in Table 1

Azoarcus evansii [20]. This suggests that component **2** consists of two $Fe^{2.5+}$ ions that are coupled via double exchange [21] resulting in a spin of $S_1 = 9/2$ which is coupled antiferromagnetically to the Fe^{3+} ion representing component **1** with $S_2 = 5/2$ resulting in a total spin of $S = 2$ [15]. This interpretation is in line with the 1:2 ratio of component **1** and **2**. Furthermore

Table 1 Mössbauer parameters of *Mt* Fdx at $T = 4.2$ K compared to the reduced form of *Dg* Fdx II at $T = 4.2$ K [10, 15]

	Mt Fdx		*Dg* Fdx II [10, 15]	
component	1	2	1	2
δ (mms^{-1})	0.27 (±0.02)	0.44 (±0.02)	0.32	0.46
ΔE_Q (mms^{-1})	−0.53 (±0.03)	1.47 (±0.03)	−0.52	1.47
Γ (mms^{-1})	0.33* (±0.02)	0.33* (±0.02)	–	–
η	−2 (±0.2)	0.4 (±0.2)	−2	0.4
D (cm^{-1})	−1.70 (±0.1)	−1.70 (±0.1)	−2.5	−2.5
E/D	0.33 (−0.05)	0.33 (−0.05)	0.23	0.23
$A/\mu NgN$ (T)	(116120129) (±5)	(−140–140 -126) (±5)	(99116126)	(−149–149 -116)
% Area	33	67	33	67

* For the simulation of the spectrum at $T = 77$ $\Gamma_1 = 0.30$ mms^{-1} and $\Gamma_2 = 0.35$ mms^{-1} was used

the experimentally obtained hyperfine parameters are in a good agreement to the Mössbauer parameters reported for [3Fe-4S]^0-clusters [15, 17, 18, 20]. Hence, we conclude that in as isolated *Mt* Fdx CNL73887.1 more than 95% of the [3Fe-4S] clusters are in the reduced form.

The results of the calculated Mössbauer parameters are listed in Table 2. A comparison of experimentally obtained and calculated Mössbauer parameters (see Table 2) allows the assignment of iron **A** and **B** to component **2** and iron **C** to component **1**. The calculated isomer shifts represent the experimentally obtained values within the experimental error (see Tables 1 an 2). The deviation between calculation and experiment is more pronounced for the quadrupole splittings. However a comparison of the average value of ΔE_Q for iron **A** and **B** (see Table 2) and the experimentally obtained ΔE_{Q2} underlines that there is a reasonable agreement between experiment and calculation. Prior to embedding the *Rp* Fdx crystal structure in an explicit solvent box, both the structural optimization and the calculation of Mössbauer parameters were conducted for *Rp* Fdx in vacuum. However, the optimization led to a considerable structural deviation of the peripheral regions of the protein from the crystal structure (see Fig. S1). In order to create a suitable protein environment *Rp* Fdx was integrated into a box filled with water molecules with frozen coordinates for the water molecules at the edges of the box. Figure S2 shows that upon embedding *Rp* Fdx in a solvent box the overall structure of the protein is maintained during optimization. Furthermore the accordance of calculated and experimentally obtained hyperfine parameters is significantly improved for the calculation in the box compared to the calculation in vacuum for all iron ions (see Table 2).

Table 3 contains the bonding distances between the irons **A**, **B** and **C** and the respective sulfur-ligands. For S_{Cys} the distances are given explicitly while for the bridging ligands an average over all three Fe-S^{2-} bonding distances for each iron ion is presented. For the calculation of the protein embedded in water, iron **C**, which is connected to Cys 59, exhibits the lowest Fe-S bonding distance compared to iron **A** and **B**. This behaviour is most pronounced for the distances between the iron ions and the bridging sulfur atoms (Fe-S^{2-}). Since iron **A** and **B** share one electron, they possess a formal charge of +2.5 while iron **C** has a charge of +3. For Fe^{3+} the metal-ligand covalency is stronger than for Fe^{2+} [21] resulting in the observed decrease in bond distance for iron **C** and the respective sulfide anions than for iron **A** and **B**. The calculated Fe-Fe distances shown in Table 3 indicate that the ferromagnetically coupled irons **A** and **B** are significantly closer to each other than to iron **C**, which is coupled antiferromagnetically to the **A**/**B** pair. The bonding distances calculated for the protein in vacuum deviate strongly from the results found for the protein embedded in water (see Table 3). There is no discernible connection between bonding distances and oxidation state of the iron ions neither for the Fe-S nor for the Fe-Fe distances. Several Fe-S and some Fe-Fe distances extracted from the calculated structure show slight (< 0.15 Å) deviations from the X-ray crystal structure data (see Table S1). Since the X-ray crystal structure was determined for the [3Fe-4S]^0-state [3], this behaviour cannot be attributed to the redox state of the cluster. The fact that the crystal structure was obtained at pH 8.5 [3] could explain this observation since an

Table 2 Comparison of experimentally obtained and calculated Mössbauer parameters

Model	Iron	A	B	Average (A, B)	Component 2 (exp.)	C	Component 1 (exp.)
Protein in waterbox	δ (mms^{-1})	0.42	0.44	0.43	0.44	0.29	0.27
	ΔE_Q (mms^{-1})	1.43	1.67	1.55	1.47	−0.48	−0.53
Protein only	δ (mms^{-1})	0.47	0.38	0.43	0.44	0.33	0.27
	ΔE_Q (mms^{-1})	1.95	1.52	1.73	1.47	−0.66	−0.53

Table 3 Calculated Fe-S and Fe-Fe distances given in Å

Model	Fe	S_{Cys}	average S^{2-}	A	B	C
Protein in waterbox	**A**	2.392	2.308	–	2.595	2.672
	B	2.430	2.323	2.595	–	2.696
	C	2.361	2.263	2.672	2.696	–
Protein only	**A**	2.415	2.326	–	2.695	2.652
	B	2.372	2.269	2.695	–	2.680
	C	2.413	2.303	2.652	2.680	–

adjustment of the pH-value was not considered in the calculations and bonding distances in [3Fe-4S]-clusters were shown to vary slightly with the pH-value [23].

Figure 2 shows the structure of *Rp* Fdx (pdb: 4OV1) embedded in a solvent box of water as obtained after quantum chemical geometry optimization. Moreover, the electric field gradient (EFG) tensors calculated at the position of each iron nucleus are visulized with their respective orientation in the molecular coordinate system. For iron **A** and **B** $\vec{V}_{yy}$ and $\vec{V}_{zz}$ show a pronounced contribution to the EFG-tensor while the amount of $\vec{V}_{xx}$ is smaller but recognizable in both cases. For iron **C** the magnitude of the EFG tensor components are significantly smaller than for iron **A** and **B** (see Table S2).

To summarize, it was shown that in *Mt* Fdx CNL73887.1 only [3Fe-4S]- and no [4Fe-4S]-clusters are present which is in agreement to former Electron Paramagnetic Resonance studies of the oxidized form of *Mt* Fdx Rv0763c and *Mt* Fdx Rv1786 [2, 4]. From the data obtained with Mössbauer spectroscopy we conclude that as isolated *Mt* Fdx CNL73887.1 contains more than 95% reduced $[3Fe\text{-}4S]^{0}$-clusters since there was no evidence of the oxidized $[3Fe\text{-}4S]^{1+}$-form. DFT calculations of the *Rp* Fdx X-ray crystal structure embedded in a cubic box of water led to an improved reproduction of the experimentally obtained Mössbauer parameters compared to the calculation of *Rp* Fdx in vacuum. A significant influence of the iron

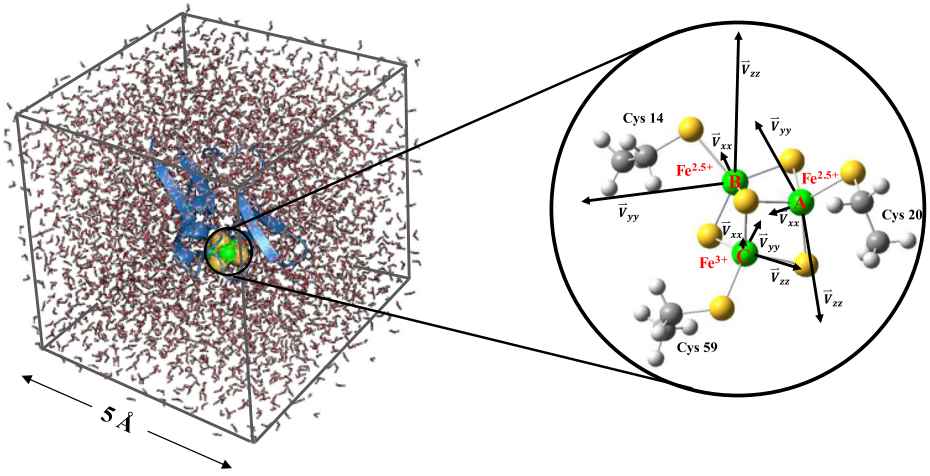

Fig. 2 Structure of *Rp* Fdx (pdb: 4OV1) visualized with PyMOL [24] embedded in a cubic box of water after geometry optimization, the iron atoms **A** to **C** are labelled in red with their formal charges. The respective Cys ligands are identified in black. The EFG tensor components $\vec{V}_{xx}$, $\vec{V}_{yy}$ and $\vec{V}_{zz}$ calculated at the position of each iron nucleus are also visualized and labelled accordingly

oxidations states on the electronic structure at the iron nuclei was illustrated by a diagram showing the orientation of the EFG tensors in relation to the cluster. Furthermore the impact of the iron oxidations states on the entire cluster-structure was detected and quantified by determination of the Fe-Fe as well as the Fe-S distances. The combination of Mössbauer spectroscopy and DFT calculations revealed that Cys 59 binds the Fe^{3+}-ion, while the $Fe^{2.5+}$-ions bound to Cys 14 resp. 20 share a delocalized electron. This information is not accessible via NMR due to the fact that the signal from $[3Fe\text{-}4S]^0$-clusters is broadened and shifted too far to be detected [25].

We aim to further improve the correlation of the experimentally obtained and calculated Mössbauer parameters by applying the ONIOM method to the X-ray crystal structures of other FeS-containing proteins, such as the *Thermus thermophilus* Rieske protein (*Tt* RP) [26], embedded in a box with explicit solvent molecules. Since protonation of the $[3Fe\text{-}4S]^0$-cluster present in *Azotobacter vinelandii* FdxI has been proposed [27], further studies on the effects of pH on the Mössbauer parameters of *Mt* Fdx CNL73887.1 will be carried out similar to pH-dependent studies of *Tt* RP and *Saccharomyces cerevisiae* Apd1 [26, 28]. In this context, the pH-value should also be taken into account in the DFT calculations.

Acknowledgements This work is supported by the German Research Foundation (DFG) under SPP 1927 (SCHU 1251/17-1, 2).

References

1. Johnson, D.C., Dean, D.R., Smith, A.D., Johnson, M.K.: Structure, function and formation of biological iron-sulfur clusters. Annu. Rev. Biochem. **74**, 247–281 (2005)
2. McLean, K.J., Warmen, A.J., Seward, H.E., Marshall, K.R., Girvan, H.M., Cheesman, M.R., Waterman, M.R., Munro, A.W.: Biophysical characterization of the sterol Demethylase P450 from *Mycobacterium tuberculosis*, its cognate Ferredoxin, and their interactions. Biochemistry. **45**, 8427–8443 (2006)
3. Zhang, T., Zhang, A., Bell, S.G., Wong, L.-L., Zhou, W.: The structure of a novel electron-transfer ferredoxin from *Rhodopseudomonas palustris* HaA2 which contains a histidine residue in its iron-sulfur cluster-binding motif. Acta Crystallogr. D. **70**, 1453–1464 (2014)
4. Lu, Y., Qiao, F., Li, Y., Sang, X.-H., Li, C.-R., Jiang, J.-D., Yang, X.-Y., You, X.-F.: Recombinant expression and biochemical characterization of *Mycobacterium tuberculosis* 3Fe-4S ferredoxin Rv1786. Appl. Microbiol. Biotechnol. **101**, 7201–7212 (2017)
5. Child, S.A., Bradley, J.M., Pukala, T.L., Svistunenko, D.A., Le Brun, N.E., Bell, S.G.: Electron transfer ferredoxins with unusual cluster binding motifs support secondary metabolism in many bacteria. Chem. Sci. **9**, 7948–7957 (2018)
6. Ouellet, H., Johnston, J.B., Ortiz de Montellano, P.R.: The *Mycobacterium tuberculosis* cytochrome P450 system. Arch. Biochem. Biophys. **493**, 82–95 (2010)
7. Poupin, P., Ducrocq, V., Hallier-Soulier, S., Truffaut, N.: Cloning and characterization of the genes encoding a cytochrome P450 (PipA) involved in Piperidine and Pyrrolidine utilization and its regulatory protein (PipR) in *Mycobacterium smegmatis* mc^2155. J. Bacteriol. **181**, 3419–3426 (1999)
8. Sielaff, B., Andreesen, J.R., Schräder, T.: A cytochrome P450 and a ferredoxin isolated from *Mycobacterium* sp. strain HE5 after growth on morpholine. Appl. Microbiol. Biotechnol. **56**, 458–464 (2001)
9. Gunnlaugsson, H.: Spreadsheet based analysis of Mössbauer spectra. Hyperfine Interact. **237**, 79–85 (2016)
10. Schünemann, V., Winkler, H.: Structure and dynamics of biomolecules studied by Mössbauer spectroscopy. Rep. Prog. Phys. **63**, 263–353 (2000)
11. Berendsen, H., van der Spoel, D., van Drunen, R.: GROMACS: a message-passing parallel molecular dynamics implementation. Comput. Phys. Commun. **91**, 43–56 (1995)
12. Neese, F.: The ORCA program system. WIREs Comput. Mol. Sci. **2**, 73–78 (2012)
13. Frisch, M. J., et al.: Gaussian 16, Revision A.03, Gaussian, Inc., Wallingford CT (2016)
14. Svensson, M., Humbel, S., Froese, R.D.J., Matsubara, T., Sieber, S., Morokuma, K.: ONIOM**:** A Multilayered Integrated MO + MM Method for Geometry Optimizations and Single Point Energy

Predictions. A Test for Diels−Alder Reactions and $Pt(P(t\text{-}Bu)_3)_2 + H_2$ Oxidative Addition. J. Phys. Chem. **100**, 19357–19363 (1996)
15. Papaefthymiou, V., Girerd, J.-J., Moura, I., Moura, J.J.G., Münck, E.: Mössbauer study of *D. gigas* ferredoxin II and spin-coupling model for Fe3S4 cluster with valence delocalization. J. Am. Chem. Soc. **109**, 4703–4710 (1987)
16. Pandelia, M.E., Lanz, N.D., Booker, S.J., Krebs, C.: Mössbauer spectroscopy of Fe/S proteins. Biochim. Biophys. Acta. **1853**, 1395–1405 (2015)
17. Huynh, B.H., Moura, J.J.G., Moura, I., Kent, T.A., LeGall, J., Xavier, A.V., Münck, E.: Conversion of [3Fe-3S] into [4Fe-4S] clusters in a Desulfovibro gigas ferredoxin and isotropic labelling of iron-sulfur cluster subsites. J. Biol. Chem. **255**, 3242–3246 (1980)
18. Emptage, M.H., Kent, T.A., Huynh, B.H., Rawlings, J., Orme-Johnson, W.H., Münck, E.: On the nature of the Iron-sulfur centers in a Ferredoxin from Azotobacter vinelandii. J. Biol. Chem. **255**, 1793–1796 (1980)
19. Gütlich, P., Bill, E., Trautwein, A.X.: Mössbauer Spectroscopy and Transition Metal Chemistry. Springer Verlag, Berlin (2011)
20. Rather, L.J., Bill, E., Ismail, W., Fuchs, G.: The reducing component BoxA of benzoyl-coenzyme A epoxidase from *Azoarcus evansii* is a [4Fe–4S] protein. Biochim. Biophys. Acta. **1814**, 1609–1615 (2011)
21. Noodleman, L., Lovell, T., Liu, T., Himo, F., Torres, R.A.: Insights into properties and energetics of iron–sulfur proteins from simple clusters to nitrogenase. Curr. Opin. Chem. Biol. **6**, 259–273 (2002)
22. GaussView, Version 6.1, Roy Dennington, T. A. Keith, J. M. Millam, Semichem Inc., Shawnee Mission, KS (2016)
23. Sykes, A.G., Cammack, R.: Advances in Inorganic Chemistry: Iron-Sulfur Proteins. Academic Press, San Diego (1999)
24. The PyMOL Molecular Graphics System, Version 2.0 Schrödinger, LLC
25. Banci, L., Camponeschi, F., Ciofi-Baffoni, S., Piccioli, M.: The NMR contribution to protein–protein networking in Fe–S protein maturation. J. Biol. Inorg. Chem. **23**, 665–685 (2018)
26. Müller, C.S., Auerbach, H., Stegmaier, K., Wolny, J.A., Schünemann, V., Pierik, A.J.: Mössbauer spectroscopy and DFT calculations on all protonation states of the 2Fe-2S cluster of the Rieske protein. Hyperfine Interact. **238**, 101–108 (2017)
27. Stout, C.D.: Crystal structures of oxidized and reduced Azotobacter vinelandii ferredoxin at pH 8 and 6. J. Biol. Chem. **268**, 25920–25927 (1993)
28. Stegmaier, K., Blinn, C.M., Bechtel, D.F., Greth, C., Auerbach, H., Müller, C.S., Jakob, V., Reijerse, E.J., Netz, D.J.A., Schünemann, V., Pierik, A.J.: Apd1 and Aim32 are prototypes of bis-histidinyl-coordinated non-Rieske [2Fe-2S] proteins. J. Am. Chem. Soc. **141**, 5753–5765 (2019)

Affiliations

Christina S. Müller[1] · Dominique F. Bechtel[2] · Hendrik Auerbach[1] · Juliusz A. Wolny[1] · Antonio J. Pierik[2] · Volker Schünemann[1]

[1] Department of Physics, Technische Universität Kaiserslautern, Erwin-Schrödinger-Str. 46, 67663 Kaiserslautern, Germany

[2] Department of Chemistry, Technische Universität Kaiserslautern, Erwin-Schrödinger-Str. 54, 67663 Kaiserslautern, Germany